Ferroelectric size effects in multiferroic $BiFeO_3$ thin films

Y. H. Chu,[a] T. Zhao, M. P. Cruz,[b] Q. Zhan, P. L. Yang, L. W. Martin, M. Huijben, C. H. Yang, F. Zavaliche, H. Zheng, and R. Ramesh
Department of Materials Science and Engineering, University of California, Berkeley, California 94720 and Department of Physics, University of California, Berkeley, California 94720

(Received 2 April 2007; accepted 30 May 2007; published online 20 June 2007)

Ferroelectric size effects in multiferroic $BiFeO_3$ have been studied using a host of complementary measurements. The structure of such epitaxial films has been investigated using atomic force microscopy, transmission electron microscopy, and x-ray diffraction. The crystal structure of the films has been identified as a monoclinic phase, which suggests that the polarization direction is close to ⟨111⟩. Such behavior has also been confirmed by piezoforce microscopy measurements. That also reveals that the ferroelectricity is down to at least 2 nm. © *2007 American Institute of Physics*. [DOI: 10.1063/1.2750524]

The magnetoelectric effect in multiferroics has attracted much attention because of the intriguing science underpinning this phenomenon.[1–4] $BiFeO_3$ (BFO) is a room temperature, single-phase, multiferroic material with a high ferroelectric Curie temperature (~1103 K) and antiferromagnetic Néel temperature (~643 K).[5,6] Understanding of the ferroelectricity in BFO, however, is still limited, especially when the vertical and lateral dimensions are reduced. Bea *et al.* have shown ferroelectric switching in BFO films down to 2 nm in thickness using piezoforce microscopy[7] (PFM) and Saito *et al.* have mapped out the structural evolution of BFO as a function of thickness.[8] There has been no literature, however, addressing the evolution of the crystal structure, ferroelectric domain structure, and ferroelectric properties as film thickness is reduced. In this study, we have probed the thickness dependence of these properties in BFO.

Films ranging from 2 to 600 nm were grown by pulsed laser deposition at 700 °C in an oxygen partial pressure of 100 mTorr on (001) $SrTiO_3$ (STO) and (110) $DyScO_3$ (DSO) substrates. A conducting $SrRuO_3$ (SRO) layer was used as a bottom electrode. The crystallinity of the BFO films was studied by x-ray diffraction (XRD) (Panalytical X'Pert MRD Pro) and scanning transmission electron microscopy (STEM) (Philips CM300 with a point resolution of 1.7 Å and information resolution of 0.8 Å and a FEI Tecnai F20 equipped with a high-angle annular dark-field detector). Surface morphology and local piezoelectric properties were investigated using an atomic force microscope (AFM)-based setup.[9] The tips used for PFM imaging were Pt/Ti coated, and had a nominal elastic constant of 4.5 N/m, and a resonance frequency of 150±30 kHz. The scanning speed was 0.6 μm/s, force applied was 100 nN, ac excitation frequency was 6.39 kHz, and the ac amplitude was 0.5 V_{pp}.

Previous studies have suggested that growth mode affects the quality and domain structure of the BFO/SRO films.[9] Figure 1(a) is an AFM image of a SRO/BFO/SRO heterostructure. The clear surface steps confirm the high-quality growth of these films. The highly crystalline nature of the BFO film is confirmed by high-resolution TEM imaging [Fig. 1(b)] and the *Z*-contrast, low magnification STEM images of a 3 nm thick BFO film [Fig. 1(c)]. The thin films also exhibit good continuity and the smooth interfaces extend throughout the entire film. The interfaces between SRO and BFO are sharp and flat, identified as dashed lines in the high-resolution image [Fig. 1(b)].

The structure of bulk BFO is characterized by two distorted perovskite unit cells (a_r=3.96 Å and α_r=0.6°) connected along their body diagonal, denoted as the pseudocubic ⟨111⟩, to build the rhombohedral unit cell.[10] Figure 2(a) shows XRD $\theta-2\theta$ scans for BFO films of varying thickness on STO substrates. Similar XRD results were also obtained for BFO films grown on DSO substrates. The out-of-plane lattice parameter, as determined from the 002 diffraction peak, is plotted in Fig. 2(b) as a function of thickness on both STO and DSO substrates. Lattice mismatch between BFO and STO (a_{STO}=0.390 nm) results in an in-plane isotropic compressive strain that causes an elongation in the out-of-plane direction; this strain gradually decreases with increasing film thickness. For films thinner than ~30 nm, the lattice parameters reach a maximum value implying that a fully epitaxial and maximally strained film has been created. On the contrary, due to the small lattice mismatch between BFO and DSO (a_{DSO}=0.395 nm), the out-of-plane lattice parameter remains closer to the bulk value over the range of thick-

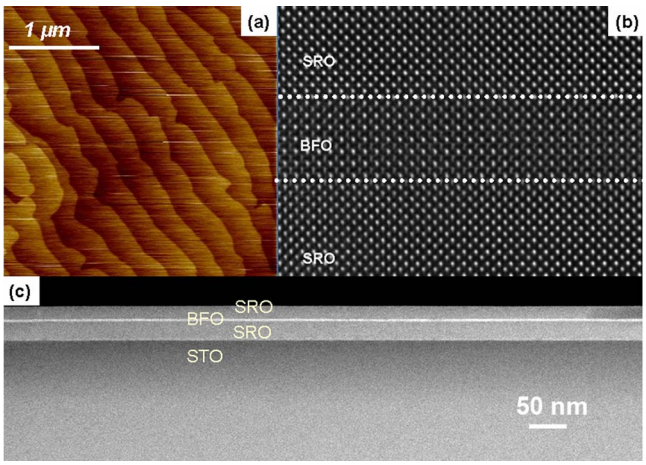

FIG. 1. (Color online) (a) AFM image of a SRO/BFO/SRO heterostructure, and typical (b) high magnification and (c) low magnification *Z*-contrast STEM images of a 3 nm thick BFO film.

[a]Electronic mail: yhchu@lbl.gov
[b]On leave from: Centro de Ciencias de la Materia Condensada, Universidad Nacional Autónoma de México, Ensenada, B.C. 22800, Mexico.

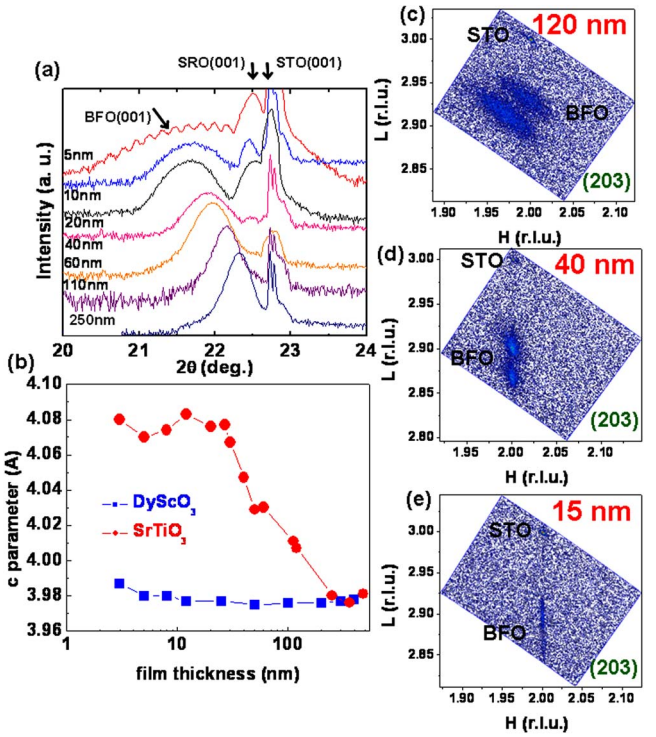

FIG. 2. (Color online) (a) XRD θ-2θ scans for the BFO films of varying thickness on STO substrates and (b) out-of-plane lattice parameter as a function of thickness on STO and DSO substrates. Reciprocal space maps (RSMs) represented in reciprocal lattice units for (c) 120, (d) 40, and (e) 15 nm BFO films [a sharp substrate peak is located at (203) position].

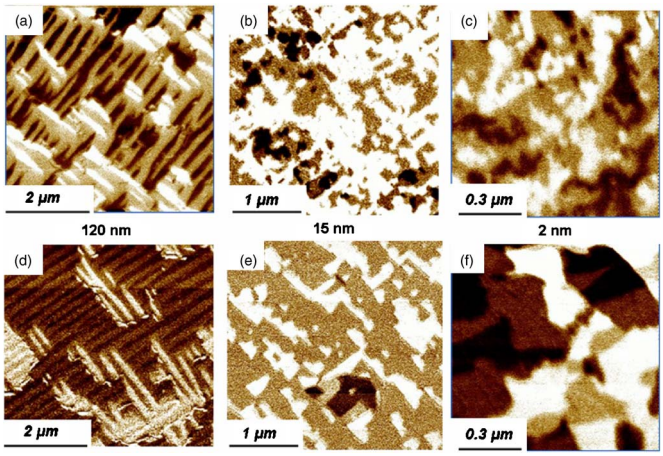

FIG. 3. (Color online) In-plane PFM images measured on (a) 120, (b) 15, and (c) 2 nm thick BFO samples on STO and in-plane PFM images measured on (d) 120, (e) 15, and (f) 2 nm thick BFO samples on DSO substrates.

nesses studied here. The lattice mismatch between BFO and the substrates also manifests itself in the crystallinity of the films. The full width at half maximum values of the XRD rocking curves of the BFO 002_{PC} diffraction peak show a range of 0.012°–0.034° and 0.12°–0.55° for films on DSO and STO substrates, respectively.

From the XRD results it is clear that 20–40 nm is a critical thickness below which the BFO films on STO are fully strained and above which the strain progressively relaxes. To fully understand the structure of the BFO films, XRD reciprocal space mapping (RSM) was employed. There are several papers addressing the structure change as a function of thickness by using RSM.[8,11,12] Previous reports focused on the 104_{PC} or 103_{PC} to identify the crystal structure of BFO; 40–70 nm was found as a critical thickness for a change in crystal structure. In order to resolve this, the 203_{PC} diffraction peak was selected because it possesses in-plane directional information necessary to give us a signature of the true crystal symmetry. In the case of films grown on STO(001), the compressive strain from the STO substrate reduces the rhombohedral symmetry ($R3c$) of bulk BFO to monoclinic, which has been used as our structural model.[13,14] In this monoclinic structure, the peak positions of the {203} reciprocal lattice reflections are shifted upward and downward, respectively, along the L direction from the pseudotetragonal position.[14] Figures 2(c)–2(e) show RSMs for BFO films of varying thickness. The in-plane positions of the 203_{PC} BFO peaks remain almost identical to that of the substrate indicating that the films are fully strained at thicknesses of 30 nm and below [Fig. 2(e)], consistent with the out-of-plane data. For the 40 nm samples, we observed clear splitting of the 203_{PC} BFO peaks; both upward and downward peaks can be detected together on the single RSM, owing to the four-variant twinlike domain structure.[9] The splitting between the two peaks yields the monoclinic angle and distortion direction to be ~0.7° along the [110]. However, the splitting of the 203_{PC} peak in the 15 nm thick BFO film is not clear. We argue that this is due to the broad peak along the L direction and the resolution limits of the x-ray optics. The 120 nm thick film also exhibits peak splitting, indicating a symmetry lower than tetragonal. The in-plane (H direction) position of the 203_{PC} peaks becomes smaller values while the out-of-plane (L direction) position becomes larger. This suggests that the structure is more similar to the bulk through strain relaxation. It is hard to argue definitively, however, that this film is fully relaxed and has reverted to the rhombohedral structure by investigating a restricted number of peaks. Moreover the lattice parameters are still slightly different from bulk values, as shown in Fig. 2(b). Additionally in this film we observed peak broadening along the perpendicular scan and different in-plane positions for the two split peaks. These are attributed to strain relaxation at this thickness, which is consistent with the rocking curve data. The structural information we obtained is different from previous reports. In order to resolve this discrepancy, identifying the polarization direction of our BFO films is crucial.

Ferroelectricity in bulk BFO is realized by a large displacement of the Bi ions relative to the FeO_6 octahedra; therefore, the ferroelectric polarization in BFO lies along the body diagonals ($\langle 111 \rangle$), and the direction of the polarization can be changed by 71°, 109°, and 180° switching.[9] However, if the structure were tetragonal, the polarization direction would be expected to be along $\langle 001 \rangle$. In the monoclinically distorted rhombohedral case, the polarization direction will likely be close to $\langle 111 \rangle$.[15] Based on this, we can interpret the polarization information we obtained from the PFM measurements. Figures 3 show in-plane PFM images measured on BFO films of varying thickness. PFM has been widely used to analyze the ferroelectric polarization direction and domain structure in BFO films.[9] Clearly three different tones, namely, white, black, and brown, can be found in these images. These three tones for the in-plane PFM images are typical for all BFO films measured along $\langle 110 \rangle$. If the cantilever is tilted off the $\langle 110 \rangle$ axes, the in-plane polarization components corresponding to the four variants will all have different finite components normal to the cantilever. By com-

paring out-of-plane (not shown) and in-plane PFM images, we can determine the ferroelectric domain structure in the BFO films. For all films, the out-of-plane and in-plane PFM images can be explained only in the confines of the monoclinically distorted rhombohedral structure. From theoretical predictions[16] and experimental observations,[17] the ferroelectric domain size in rhombohedral ferroelectrics increases with the film thickness as is observed in our study. For the 150 nm BFO films [Fig. 3(a)], stripe domain structures are observed. However, thinner BFO films (<30 nm) showed dramatically different domain morphologies [Figs. 3(b) and 3(c)]. In the rhombohedral structure, there are two contributions to the elastic energy: normal strain caused by lattice mismatch and shear strain caused by the rhombohedral symmetry.[18] These terms are proportional to the film thickness; however, the normal strain energy can be released by forming dislocations when film thickness increases. The shear strain energy goes up when we increase the thickness and, therefore, thicker films exhibit well defined domain patterns. Upon decreasing the BFO thickness (2 nm), we observed the domain size of BFO films on DSO [Fig. 3(f)] to be larger than BFO films on STO. Such a difference arises from the normal strain since it cannot be released at such thicknesses; therefore, BFO films on STO have larger elastic strain energy, which leads to smaller domain structures.

In films thicker than ~100 nm, square piezoelectric hysteresis loops are observed with a d_{33} value of 60 pm/V. Below ~50 nm, it becomes increasingly difficult to quantitatively measure the ferroelectric/piezoelectric properties in a capacitor geometry due to a progressively larger contribution from leakage. In order to overcome this problem, we have used the PFM tip as the top electrode to locally probe the piezoelectric hysteresis. In such measurements, both amplitude and phase information were acquired simultaneously to gain insight into the strength and switchability of the ferroelectric order. At such small thicknesses (i.e., below ~10 nm), the amplitude data are highly convoluted by parasitic effects; however, the corresponding phase hysteresis data clearly illustrate the existence of ferroelectric switching, manifested as a 180° change in the phase angle of the lock-in system. Figures 4(a)–4(d) are piezoelectric response phase loops for the BFO films with different thicknesses. These data indicate that all of the samples, down to a thickness of 2 nm, i.e., five BFO unit cells, are switchable by an electrical field. However, the asymmetry of the coercive field was observed for all the samples; this is due to a self-poling effect, which arises at the interface between BFO and bottom electrode. Since the projection of the polarization is downward, it suggests that this state is more stable compared to a corresponding upward state. Moreover, the coercive field increases significantly as the thickness is reduced.

In conclusion, we have deposited fully epitaxial BFO films on STO(001) and DSO(110) substrates with SRO bottom electrode layers with thicknesses ranging from 2 to 600 nm. The resulting high quality of the BFO films has been verified by AFM, TEM, and XRD. The crystal structure of the BFO films has been identified as monoclinic, which suggests that the polarization direction is close to ⟨111⟩. These behaviors have also been confirmed by PFM. The BFO films showed ferroelectric response down to 2 nm.

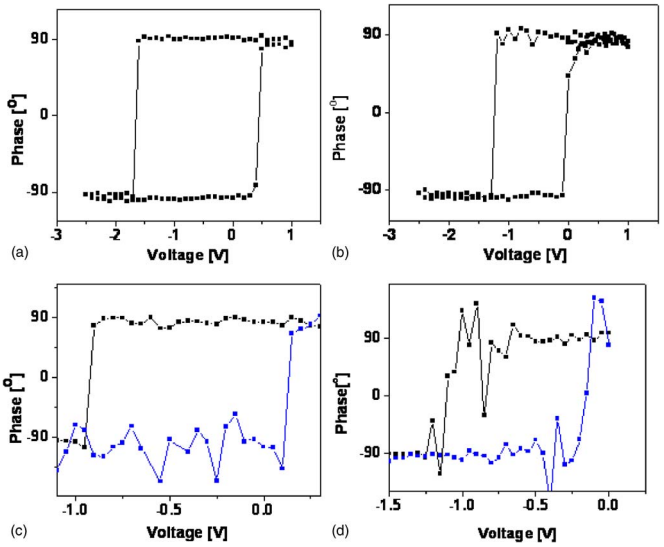

FIG. 4. (Color online) Piezoelectric response phase loops for (a) 30, (b) 8, (c) 4, and (d) 2 nm BFO films on STO substrates.

The authors thank useful discussions with L. Q. Chen and J. X. Zhang in Penn State University. This work was supported by the Director, Office of Science, Office of Basic Energy Sciences, Materials Sciences and Engineering Division, of the U.S. Department of Energy under Contract No. DE-AC02-05CH11231; and by the Office of Naval Research under ONR Grant No. N00014-06-1-0008 and ONR-MURI Grant No. E-21-6RU-G4. The authors acknowledge support of the National Center for Electron Microscopy, Lawrence Berkeley National Laboratory.

[1] Y. Tokura, Science **312**, 1481 (2006).
[2] R. Ramesh and N. A. Spaldin, Nat. Mater. **6**, 21 (2007).
[3] W. Eerenstein, N. D. Mathur, and J. F. Scott, Nature (London) **442**, 759 (2006).
[4] N. A. Spaldin and M. Fiebig, Science **309**, 391 (2005).
[5] P. Fischer, M. Połomska, I. Sosnowska, and M. Szymański, J. Phys. C **13**, 1931 (1980).
[6] C. Michel, J. M. Moreau, G. D. Achenbechi, R. Gerson, and W. J. James, Solid State Commun. **7**, 701 (1969).
[7] H. Bea, S. Fusil, K. Bouzehouane, M. Bibes, M. Sirena, G. Herranz, E. Jacquet, J. P. Contour, and A. Barthelemy, Jpn. J. Appl. Phys., Part 2 **45**, L187 (2006).
[8] K. Saito, A. Ulyanenkov, V. Grossmann, H. Ress, L. Bruegemann, H. Ohta, T. Kurosawa, S. Ueki, and H. Funakubo, Jpn. J. Appl. Phys., Part 1 **45**, 7311 (2006).
[9] F. Zavaliche, S. Y. Yang, T. Zhao, Y. H. Chu, M. P. Cruz, and R. Ramesh, Phase Transitions **79**, 991 (2006).
[10] F. Kubel and H. Schmid, Acta Crystallogr., Sect. B: Struct. Sci. **B46**, 698 (1990).
[11] D. S. Rana, K. Takahashi, K. R. Mavani, I. Kawayama, H. Murakami, and M. Tonouchi, Phys. Rev. B **75**, 060405(R) (2007).
[12] H. Bea, M. Bibes, S. Petit, J. Kreisel, and A. Barthelemy, Philos. Mag. Lett. **87**, 165 (2007).
[13] G. Xu, H. Hiraka, G. Shirane, J. F. Li, J. Wang, and D. Viehland, Appl. Phys. Lett. **86**, 182905 (2005).
[14] G. Xu, J. Li, and D. Viehland, Appl. Phys. Lett. **89**, 222901 (2006).
[15] C. Ederer and N. A. Spaldin, Phys. Rev. Lett. **95**, 257601 (2005).
[16] A. E. Romanov, M. J. Lefevre, J. S. Speck, W. Pompe, S. K. Streiffer, and C. M. Foster, J. Appl. Phys. **83**, 2575 (1998).
[17] Y. B. Chen, M. B. Katz, X. Q. Pan, R. R. Das, D. M. Kim, S. H. Baek, and C. B. Eom, Appl. Phys. Lett. **90**, 072901 (2007).
[18] N. Farag, M. Bobeth, W. Pompe, A. E. Romanov, and J. S. Speck, J. Appl. Phys. **97**, 113156 (2005).